https://doi.org/10.1016/j.conbuildmat.2020.120971

Comparative studies on passivation and corrosion behaviors of two types of steel bars in simulated concrete pore solution

Yamei Cai [a], Haibing Zheng [a, *], Xiang Hu [a], Jianxin Lu [a], Chi Sun Poon [a, *], Weihua Li [b, c]

[a] Department of Civil and Environmental Engineering, The Hong Kong Polytechnic University, Hong Kong
[b] College of Chemical Engineering and Technology, Sun Yat-sen University, Tangjiawan, Zhuhai 519082, China
[c] Institute of Oceanology, Chinese Academy of Sciences, Qingdao 266071, China

Corresponding author: cecspoon@polyu.edu.hk

Abstract: The corrosion behavior of two types of stirrups, a plain steel bar and a ribbed steel bar, were studied in this work. The results demonstrated that a better passive state was achieved on B500, which was due to a relatively higher concentration of Fe^{2+} oxides at the first 2 nm depths of the film, even though B500 film had relatively less FeO_x contents, because Fe^{2+} oxides had a better protective property than Fe^{3+} oxides. Furthermore, the slightly lower donor density of B500 film in the M-S analysis results presented the much less point defect in the film, showing an increase in the anti-corrosion property of passive film. These contributed to a higher chloride threshold value of B500, 4 times higher than that of S275. Therefore, compared with S275, B500 stirrups could be more suitable for the application in the severe service environment.

Keywords: Stirrups; Steel bars; Corrosion; Passive film; Chloride threshold value

1. Introduction

The deterioration of reinforced concrete structures due to the corrosion of steel bars needs considerable financial resources to repair and maintain annually, which has received widespread attention all over the world [1-7]. It is well known that the steel bars in concrete structural members, such as beams and pillar, may serve as main bars and stirrups. However, previous researches mainly focused on the aspects related to the corrosion of main bars, usually ribbed steel bars. In fact, the stirrups would be more prone to corrosion, they play a

sacrificing role in protecting the main bars from corrosion [8, 9]. As shown in the below schematic diagram (Fig.1), compared with main bars, the path for the aggressive ions, e.g. chloride ions, from the concrete surface to the stirrups is much shorter. In addition, the smaller diameter and different chemical compositions of stirrups may be other reasons for its initiation and propagation of corrosion firstly.

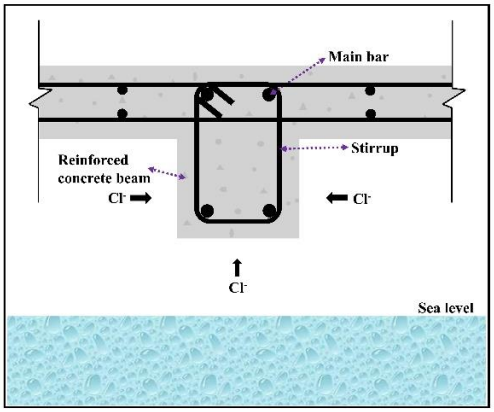

Fig. 1 Schematic diagram of main bar and stirrups in reinforced mairne concrete

The passive film formed on the surface of steel in the highly alkaline pore solution of concrete is very important in governing the service life of the concrete structures. The chemical composition of steel matrix can affect the constitution and stability of passive film. It has been reported that the passive film of carbon steel had a bilayer structure; the inner layer was mainly composed of Fe^{2+} oxides, while the outer layer was primarily made up of Fe^{3+} oxides [10, 11]. Compared with Fe^{3+} oxides, Fe^{2+} oxides may have a better protective property against corrosion [11, 12]. As a result, steel bars with different chemical compositions may form passive films with different amount of Fe^{2+} or Fe^{3+} oxides. This could be one of the reasons why the properties of corrosion resistance has huge difference in different types or grades of steel. Nowadays, extensive research primarily focused on the improvement in the stability of passive film and anti-corrosion properties of newly developed main bars (i.e. new composition or surface-treated steel) [12-17]. Few research studies were about the assessment of corrosion-resistance property of stirrups and the selection of stirrups according to both their anti-corrosion ability and exposure environment condition.

Generally, two types of steel bars can be used as stirrups, plain steel reinforcing bars and ribbed steel reinforcing bars. The former is usually low-priced in lower strength grade and the latter is high-priced in higher strength grade. The priority might be placed on the former when the strength requirement was fullfiled due to the economic considerations. For the marine concrete structures, corrosion resistance of the steel bar is another essential factor to be carefully considered during the design stage of the structures. However, the corrosion behaviors of these two types of steel bars were not thoroughly compared. Therefore, in this work, the anti-corroison performance, including the passivation and depassivation of these two types of steel bars were compared in the simulated concrete pore solution using open circuit potentials (OCP), electrochemical impedance spectroscopy (EIS) and linear polarization resistance (LPR) test methods. In addition, the composition and electronic properties of passive films were further analysed by X-ray photoelectron spectroscopy (XPS) and Mott-Schottky (M-S) tests. This work would be useful for the selection of stirrups types in different service environment.

2. Materials and experimental methods

2.1 Preparation of steel specimen and electrolyte

In this study, a plain steel reinforcing bar (S275J0, designated as “S275”) with a lower grade and a ribbed steel reinforcing bar (B500) with a higher grade were used to compare their passivation and anti-corrosion performances. The chemical compositions are listed in Table 1. The steel bars were cut into dimensions of Ø10 mm × 2 mm. After removal of rust, a copper wire was soldered to one end of the steel bars and the epoxy resin was used to seal the specimens, leaving a same exposed area of 0.785 cm^2. Prior to all measurements, firstly, the exposed parts of the steel bars were polished using silicon carbide paper of gradation 78 μm, 35 μm and 15 μm, respectively. Then these samples were further polished using diamond polishing fluid of gradation 9 μm and 3 μm, and alumina polishing fluid of gradation 0.05 μm. The above polishing time was 5 min for each polishing step. After that, these samples were degreased by ethanol and dried by cold flowing air. These polishing steps were adopted to

gain reproducible results, because the surface finish strongly affected the electrochemical test result [18].

A saturated $Ca(OH)_2$ (designated as CH) solution was chosen to simulate the concrete pore solution. The solution was prepared by dissolving analytical grade CH in deionized water. During the entire passivation process, the solution was tightly sealed in order to prevent from carbonation. The pH values were recorded in the initial and final passivation time, and the data was demonstrated in the Table 2.

After passivation process, analytical grade sodium chloride (used as a chloride source) was added incrementally into the solution until the corrosion initiated. Each addition amount of chloride was 0.1 mol/L (designated as "0.1 M"), and the time interval between each addition was 12 h to allow enough time for the reaction between the chloride ion and the specimens.

Table 1 Chemical compositions of the steel bars

Element	S275 (wt%)	B500 (wt%)
C	0.180	0.200
Si	0.230	0.593
Mn	0.830	1.160
Cr	0.080	0.037
Ni	0.060	0.032
Mo	0.008	0.003
Cu	0.370	0.047
Al	0.028	\
S	0.028	0.004
P	0.026	0.012
Co	\	\
N	0.008	0.008
V	\	0.004
W	0.004	\
Fe	Balance	Balance

Table 2 pH values of electrolyte in the initial and final passivation time

Item	Initial time (0 h)	Final time (336 h)
S275	12.60	12.56
B500	12.54	12.54

2.2 Electrochemical measurements

A traditional three-electrode electrochemical configuration was used in this work as demonstrated in Fig. 2. The steel specimens were used as the working electrode. The reference electrode was a saturated calomel electrode (SCE) with a Luggin capillary, and a platinum plate with an area of 1 cm^2 was used as the counter electrode. All electrochemical measurements were carried out at 22 ± 1 ºC. All the potentials of steel specimens in this work were measured with respect to SCE.

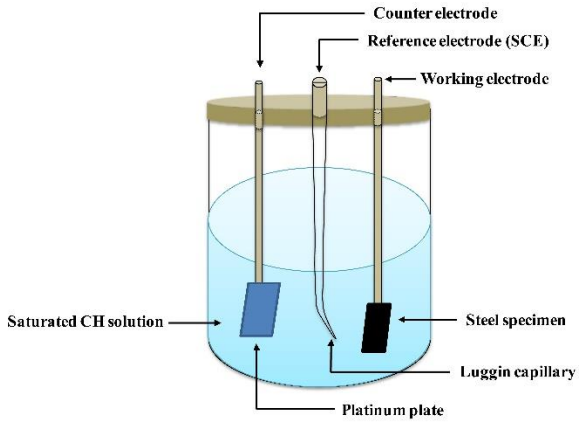

Fig. 2 Schematic diagram of three-electrode electrochemical setup

During passivation process, open circuit potentials (OCP) and electrochemical impedance spectroscopy (EIS) were monitored periodically. The EIS measurement was conducted by a Multi-Autolab M 204 device with a frequency range from 100 kHz to 10 mHz and a 10 mV AC signal magnitude. The impedance data was fitted by a ZsimpWin software. Besides, at the end of passivation period (336 h), Mott-Schottky (M-S) test was used to measure the electronic property of passive film. This test was conducted at a frequency of 1 kHz and a potential range from -1.0 to 0.6 V (*vs.* SCE), and the stepping interval and AC signal amplitude were 50 mV and 10 mV, respectively.

During depassivation process, OCP and EIS were also used to characterize the surface conditions of steel specimens periodically. In addition, Linear polarization resistance (LPR) test was periodically conducted using a scan rate of 0.167 mV/s with the potential range from -0.01 to 0.01 V (*vs.* OCP).

For each electrochemical test, three steel specimens were measured to ensure reproducibility. One representative specimen was selected and presented in the results of Section 3.

2.3 Characterization of passive film

After passivation for 336 h, the chemical composition of the passive film of steel specimens was investigated by an XPS spectrometer. All the steel specimens were ion sputtered using an Argon gun, and an in-depth profile analysis was carried out at 4 keV using an Argon ion beam with a 140 μA extractor current and a raster area of 3×3 mm. The data of XPS spectrum was fitted using a curve-fitting program of XPSPEAK 4.1.

3. Results and discussion

3.1 Passivation of steel bars

3.1.1 Evolution of open circuit potential (OCP)

Fig. 3 presents the variation of OCP values of S275 and B500 with increasing immersion time in the saturated $Ca(OH)_2$ solution. For the S275, during the first 12 h of immersion, the OCP value increased quickly from about -0.278 V to -0.210 V, and then there was a slow increase in the subsequent immersion time. The value tended to be stable at about -0.106 V after nearly 288 h of immersion. For the B500, a sharp increase by about 0.117 V was seen after 72 h of immersion, and afterwards, there was a moderate rise from -0.180 V to -0.121 V, which was similar with the potential obtained in the S275 specimen.

The OCP values of all samples shifted toward to the more positive direction with time, and then the value tended to stabilize, which was attributed to the evolution of the passive film [19]. In this data, there was a slightly lower OCP value of B500 sample compared with S275 sample, which may be related to their different chemical compositions and micro-structural characteristics of passive film caused by difference of steel matrix [13].

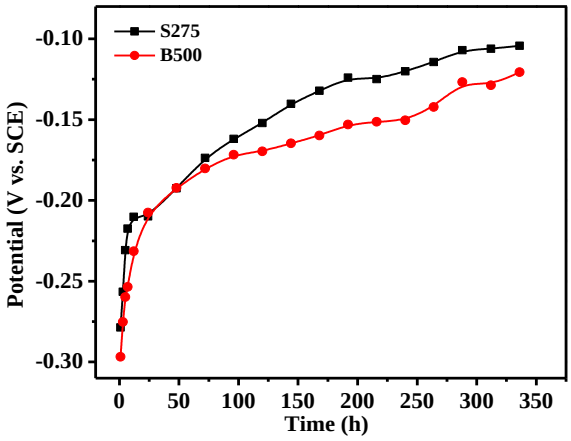

Fig. 3 Variations of open circuit potential of S275 and B500 specimens with immersion time in sat. $Ca(OH)_2$ solution

3.1.2 Electrochemical impedance spectroscopy (EIS)

Fig. 4 shows the Nyquist and Bode curves of S275 and B500 immersed in the saturated $Ca(OH)_2$ solution for different times. In the Nyquist plots of Figs. 4 (a) and (c), the radius of capacitive loop increased gradually as the immersion time increased. Meanwhile, the plateaus of the phase angles were broadened and enlarged, and the modulus value of impedance increased markedly in the Bode diagrams of Figs. 2 (b) and (d). These results showed that the passivation degree of S275 and B500 increased with the immersion time.

For S275, in Figs.4 (a) and (b), from the first 1 h to 24 h of immersion, there was a slight increase in the radius of capacitive loop, a marginal broadening in the plateaus of the phase angles and a moderate rise in the modulus value of the impedance. From 24 h to 168 h of immersion, the increasing range of these factors considerably increased. After 168 h, these factors tended to be stable. By contrast, B500 (Figs. 4 (c) and (d)) had a quick passivation process from 1 h to 72 h of immersion. And after 72 h of immersion, a relatively stable passivation rate was observed.

When compared S275 with B500, except for the immersion time of 1 h, the Nyquist and Bode curves of the S275 showed a smaller radius of capacitive loop, narrower plateaus of the phase angles and a lower modulus value of the impedance. This demonstrated that the development of passivation degree of B500 was faster than that of S275. But in very early age

(less than 1 h), S275 had a relatively quicker passivation rate, the reason will be explained in the following contents.

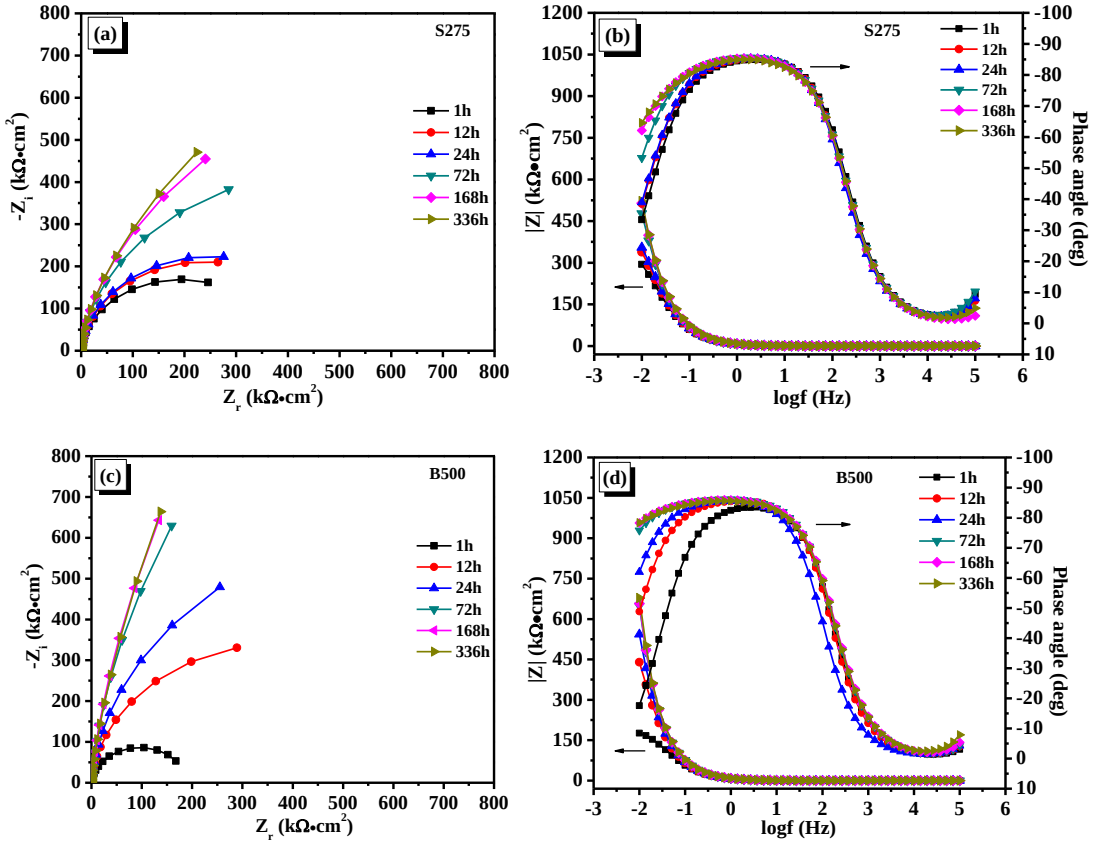

Fig. 4 Impedance spectrum in Nyquist ((a) and (c)) and Bode ((b) and (d)) curves for S275 and B500 at different immersion times of sat. $Ca(OH)_2$ solution

In order to further analyze the EIS results, the impedance data were fitted using the equivalent circuit shown in Fig. 5. In the equivalent circuit plot, R_s represents the solution resistance from the reference electrode to the working electrode, Q_{dl} denotes the capacitance of double electric layer and R_p represents the polarization resistance of the whole passive film [12, 14, 20].

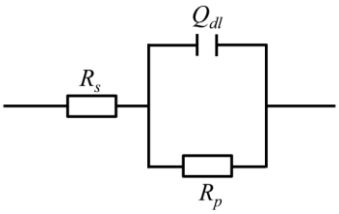

Fig. 5 Equivalent circuits used to fit the EIS results

The fitting parameters of the EIS data are shown in Table 3. For both S275 and B500, there was an increase in R_p value and decrease in Q_{dl} value with the increase of immersion time, which indicated the growth of the passive film, including the increase of the thickness and compactness [21, 22]. In addition, it was found that, at 1 h of immersion, S275 had a higher R_p value than that of B500. Afterwards, the R_p value of B500 dramatically increased and became higher. This variation trend of R_p was in line with the Nyquist plot in the Fig. 4. During the first 1 h of immersion, the rapid passivation rate of S275 could be attributed to the different chemical compositions of the steel. In comparison, the Cr content in S275 (0.08 wt%) was higher than that in B500 (0.037 wt%) as shown in table 1. It has been reported by Liu et al. [12] that Cr can inhibit the formation of the passive film at the early age, but the final thickness and stability of the passive film increased.

Table 3 Fitting results of the EIS parameters of S275 and B500

Item	Time/h	R_s ($\Omega \cdot cm^2$)	Q_{dl} ($S \cdot s^n \cdot cm^{-2}$)	n	R_p ($k\Omega \cdot cm^2$)
S275	1	36.79	2.54E-05	0.9533	355
	12	40.63	2.45E-05	0.9545	440
	24	44.42	2.39E-05	0.9558	463
	72	42.92	2.27E-05	0.9542	832
	168	47.10	2.19E-05	0.9479	1134
	336	49.59	2.12E-05	0.9432	1221
B500	1	49.02	2.51E-05	0.9451	188
	12	51.30	2.36E-05	0.9575	696
	24	81.86	2.25E-05	0.9593	1248
	72	50.71	2.09E-05	0.9569	3399
	168	50.76	2.06E-05	0.9529	4497
	336	54.53	2.00E-05	0.9495	4524

3.1.3 Chemical composition analysis of passive films

The chemical compositions of the passive films have great impacts on the anti-corrosion performance of steel. Fig. 6 shows the variation of the high resolution spectrum of Fe $2p_{3/2}$ of S275 and B500 after immersed in saturated $Ca(OH)_2$ solution for 336 h. It was reported that the passive film of carbon steel was primarily made up of Fe-oxide/hydroxide [10, 11]. According to the method reported by Ghods [10, 11], different Fe chemical states at different sputtered depths were fitted, the results are shown in Fig.6.

In Fig. 6, as expected, the peak intensity of Fe metal (Fe-1) increased with the sputtered depth. And at the depth of 5 nm, the dominated Fe state was Fe metal (Fe-1), which was associated with the steel substrate. This indicated a slight shift of the Fe $2p_{3/2}$ signal from ~713 eV to ~706 eV at sputtered depths from 0 to 5 nm, which also denmonstrated that the passive film on the surface of the steel was quite thin.

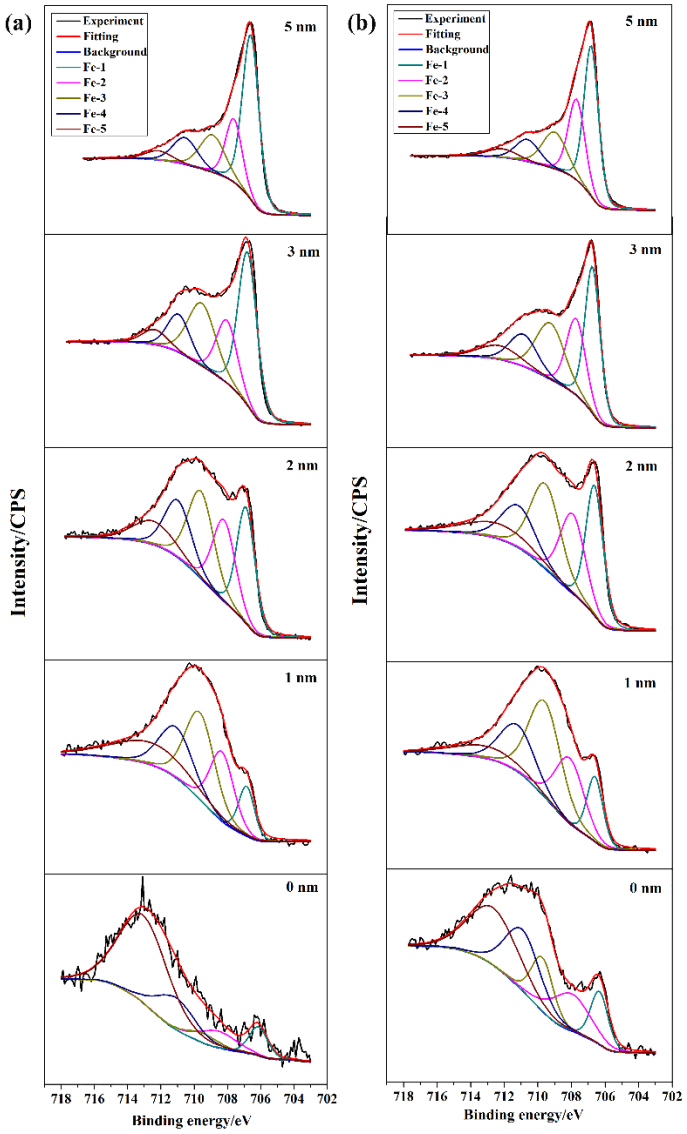

Fig. 6 Fe $2p_{3/2}$ peak fitting curves of passive film on the surface of S275 (a) and B500 (b) at different sputtered depths (Fe-1: Fe metal, Fe-2: Fe_3C, Fe-3: Fe_3O_4/FeO, Fe-4: Fe_2O_3/FeOOH, Fe-5: Fe_2O_3/FeOOH-satellite)

According to the fitting results shown in Fig. 6, the ratios of Fe oxides to Fe metal (FeO_x/Fe metal) and Fe^{2+} oxides to Fe^{3+} oxides (Fe^{2+}/ Fe^{3+}) at each sputtered depth were calculated by proportioning the total intensity of Fe oxides (i.e., Fe-3, Fe-4 and Fe-5) to the intensity of Fe metal (i.e., Fe-1) and the intensity of Fe^{2+} oxides (i.e., Fe-3) to the total intensity of Fe^{3+} oxides (i.e., Fe-4 and Fe-5), respectively. These results are shown in Fig. 7.

As shown in Figs. 7 (a) and (b), the S275 specimen had a relatively larger ratio of FeO_x/Fe metal at the first 2 nm depths of passive film than B500 (Fig. 7 (a)). However, compared with the passive film of B500, there was a relatively lower concentration of Fe^{2+} oxides in the S275 passive film at the first 2.3 nm depths (Fig. 7 (b)). Therefore, the higher Fe^{2+} oxide contents on the surface layer of B500 could contribute to a more stable passive state to protect steel from corroding, because Fe^{2+} oxides in the passive film has a better protective property than Fe^{3+} oxides [11, 23].

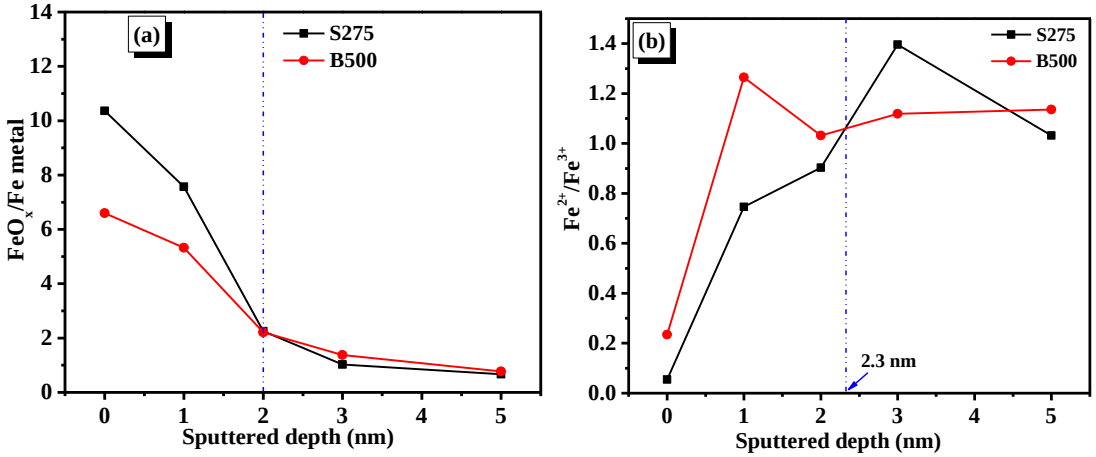

Fig. 7 Comparison of the Fe-oxides at different depths of passive film of S275 and B500: (a) is the ratio variation of FeO_x/Fe metal with the increase of the depths of passive film, and (b) is the ratio of Fe^{2+}/Fe^{3+} in the passive film

3.1.4 Semiconductor properties of the passive films

Through capacitance measurement, Mott-Schottky analysis has been proven to be a powerful tool for in-situ analysis of the passive films formed on the surface of steel specimens，and the Mott-Schottky equation is as follows [24-28]:

$$\frac{1}{C^2} = \pm \frac{2}{\varepsilon\varepsilon_0 eN}\left(E - E_{fb} - \frac{kT}{e}\right) \quad (3)$$

Where the positive sign and negative sign are for n-type and p-type conductivity, respectively, C is equal to the space charge capacitance C_{SC}, E is the applied electrode potential, E_{fb} is the flat band potential, ε is the relative dielectric constant of the passive film (12 for the Fe-oxide on the surface of carbon steel [29]), ε_0 is the vacuum permittivity (ε_0=8.85×10^{-12} F/m), e is the electron charge (e=1.602×10^{-19} C), N is the charge carried

density, the donor density (N_D) is for n-type semiconductor and the accept density (N_A) is for p-type semiconductor, k is the Boltzmann's constant (k=1.38×10^{-23} J/K), and T is the absolute temperature.

Fig. 8 shows the Mott-Schottky curves of S275 and B500 after immersed in the saturated $Ca(OH)_2$ solution for 336 h. The similar curve shapes of S275 and B500 indicated the comparable composition of their passive films. In addition, it can be seen that the curves from -0.6 V to +0.5 V showed positive slopes, which meant that the passive films behaved as n-type semiconductor [30]. However, the nonlinearity of the whole region from -0.6 V to +0.5 V could be due to the two donor levels existing in the band gap, i.e., shallow donor (region I) and deep donor (region II) [31, 32]. It has been reported that the shallow and deep levels were related to the presence of Fe^{2+} ions in tetrahedral and octahedral position, respectively [32-34].

The donor densities (N_D) of S275 and B500 can be determined from the first positive slope of C^{-2} vs. E curves in the region I, and the values are shown in Table 4. It can be seen from Table 4 that the order of magnitude of N_D was 10^{21} cm^{-3}, which was in agreement with other authors [12, 29, 35]. Besides, it was found that the donor densities of S275 passive film was slightly higher than those of B500 passive film. This may be related to different chemical composition of passive films. It has been presented in XPS results in Fig. 7 (b), there was a relatively higher tendency of oxidation reaction from Fe^{2+} to Fe^{3+} in the film of S275, this oxidation process could be seemed as the replacement of Fe^{2+} by Fe^{3+}, which could form an ionic species (Fe_{Fe}^{+}) with a charge of +1 [36]. In order to achieve charge neutrality, the density of oxygen vacancy would increase in the film. This may result in increase in donor densities of S275 passive film, which would be responsible for the high degeneracy of the passive film [37, 38].

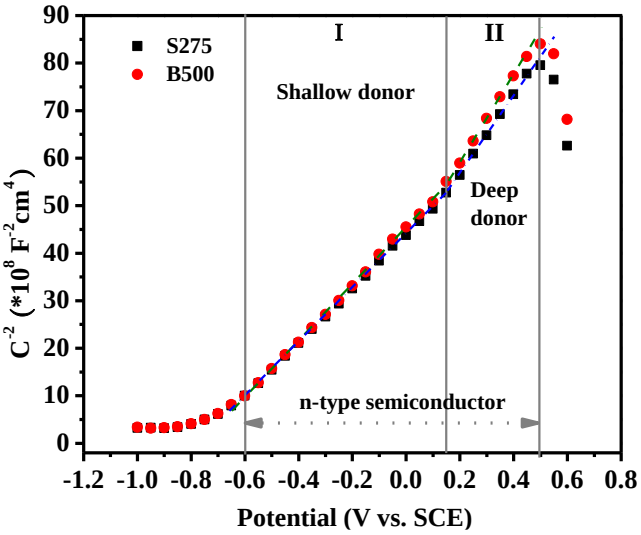

Fig. 8 Mott-Schottky curves of the passive films formed on the surface of the steel specimens after immersed in sat. $Ca(OH)_2$ solution for 336 h

Table 4 Donor densities of passive films on the surface of steel specimens after immersed in sat. $Ca(OH)_2$ solution for 336 h

Steel type	S275	B500
$N_D/10^{21}cm^{-3}$	2.06	1.97

3.2 Chloride-induced corrosion initiation of steel specimens

Open circuit potential (OCP) and linear polarization resistance (LPR) tests were conducted to monitor the corrosion initiation induced by chloride ions in the saturated $Ca(OH)_2$ solution. EIS were also used to confirm the initiation of the pitting corrosion. Fig. 9 shows the variation of OCP and LPR values as a function of chloride ion concentration for S275 and B500. Fig. 10 displays the evolution of the Nyquist plots with the concentration of chloride ions, and Table 5 shows the fitting results of EIS test using the equivalent circuit in Fig. 5.

For S275, in Fig. 9, the OCP value remained at about -0.11 V when the concentration of chloride ion was lower than 0.8 M and 0.7 M for Sample 1 (S1) and Sample 2 (S2) respectively. When the concentration of chloride ion reached 0.8 M and 0.7 M, a sharp negative shift of potential and an abrupt drop of $R_{p,LPR}$ value were observed in the plots, indicating the breakdown of the passive film and the initiation of the pitting corrosion. In

addition, at 0.8 M (S1), there were also significant decrease in both the semicircle diameter of the Nyquist plots (Fig. 10(a)) and the R_p values in the fitted results (Table 5), which confirmed the depassivation of the steel specimen. Therefore, the chloride threshold value for S275 could be conservatively defined as 0.6 M. Accordingly, B500 had a similar evolution process in the plots of OCP, LPR and EIS, its chloride threshold value could be defined as 2.6 M.

Compared with S275 and B500, the chloride threshold value of B500 was 4 times higher than that of S275, which is mainly attributed to a more stable passive state of B500, as mentioned in the above contents. Besides, the higher $R_{p,LPR}$ value of B500 represented a lower corrosion rate, which indicates a lower propagation rate of the corrosion process [39, 40]. Therefore, the use of B500 stirrups in the severe service environment would be a better choice as it has a more stable passive state and a much higher chloride threshold. The service life of the concrete structure in the aggressive environment would be significantly prolonged.

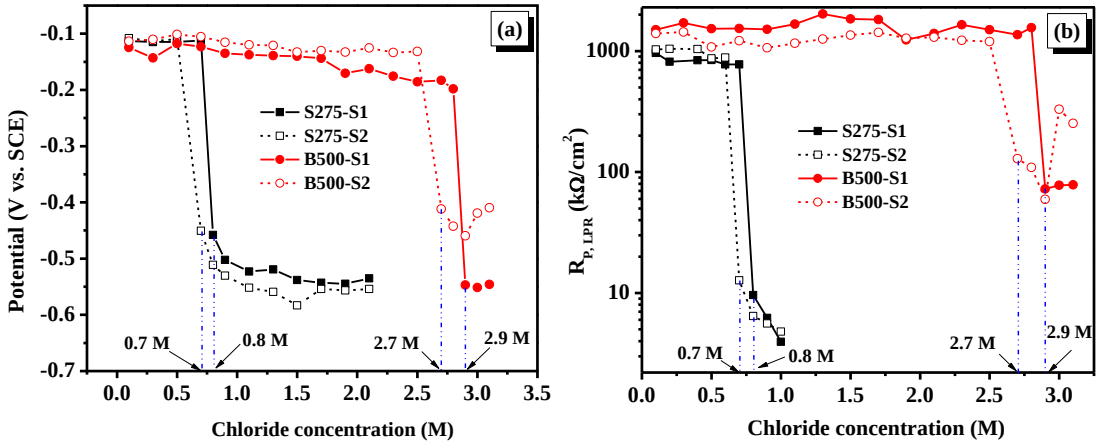

Fig. 9 Evolution of OPC (a) and LPR (b) of S275 and B500 with the increase of chloride ion concentration in sat. $Ca(OH)_2$ solution (Results of two representative specimens were presented)

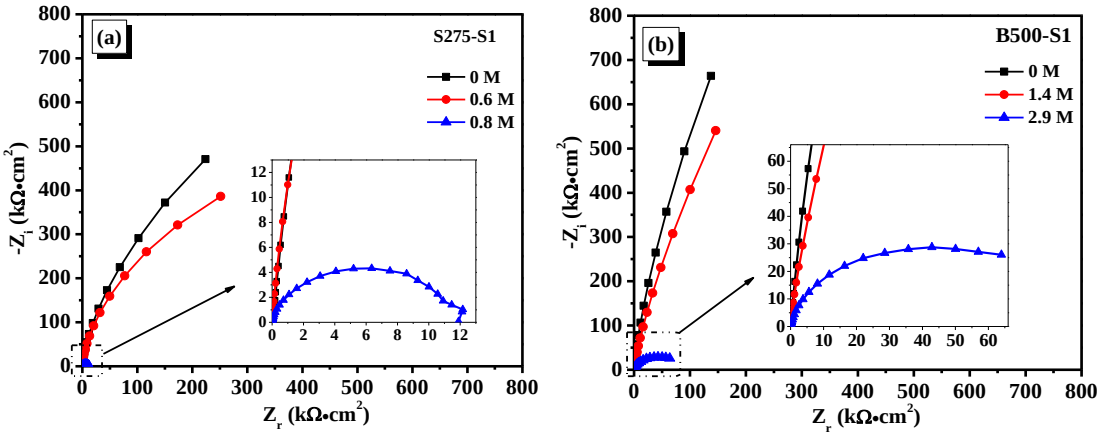

Fig. 10 Nyquist plots of S275-S1 (a) and B500-S1 (b) in sat. $Ca(OH)_2$ solution with different chloride ion concentration

Table 5 Fitting results of EIS parameters of S275-S1 and B500-S1 in sat. $Ca(OH)_2$ solution with different chloride ion concentration

Item	Cl^- concentration (mol/L)	R_s ($\Omega \cdot cm^2$)	Q_{dl} ($S \cdot s^n \cdot cm^{-2}$)	n	R_p ($k\Omega \cdot cm^2$)
S275	0	49.59	2.12E-05	0.9432	1221
	0.6	6.51	2.22E-05	0.9524	804
	0.8	11.96	4.04E-05	0.9048	11
B500	0	54.53	2.00E-05	0.9495	4524
	1.4	4.13	2.13E-05	0.9373	2348
	2.9	3.96	4.49E-05	0.8811	69

4. Conclusions

This study compared the passivation and corrosion behaviors of S275 and B500 steel reinforcing bars in the simulated concrete pore solution. From this work, the following findings can be summarized:

- The passivation rate of S275 was higher within the first 1 h immersion and became lower afterwards, this also resulted in a worse passivation state after 14 days immersion. The difference of the passivation behavior was mainly due to the chemical composition and the microstructure of the two types of steel bars.

- For S275, there was a relatively higher proportion of FeO_x but a lower proportion of Fe^{2+} oxides at the first 2 nm depths of passive film, leading to a less protective property of this passive film. The donor density of passive film of S275 was slightly higher compared with that of B500, implying that more point defects were presented in the passive film. These might be the causes of a relatively poor anti-corrosion performance of S275.
- The chloride threshold value of B500 in the saturated $Ca(OH)_2$ solution, which was closely associated with the passivation behavior, was significantly (4 times) higher than that of S275. It also showed that B500 steel reinforcing bar may be more suitable for stirrups in aggressive environment, such as marine and deicing salt environments.

Acknowledgements

The authors wish to thank the financial supports of Hong Kong Branch of National Engineering Research Center for Steel Construction through the project 1-BBYP and The Hong Kong Polytechnic University. The last author also acknowledges the support of National Natural Science Fund for Distinguished Young Scholars (51525903).

References

[1] S. Ahmad, Reinforcement corrosion in concrete structures, its monitoring and service life prediction—a review, Cem. Concr. Compos. 25(4-5) (2003) 459-471.

[2] C.A. Apostolopoulos, V.G. Papadakis, Consequences of steel corrosion on the ductility properties of reinforcement bar, Constr. Build. Mater. 22(12) (2008) 2316-2324.

[3] R.E. Melchers, C.Q. Li, Reinforcement corrosion initiation and activation times in concrete structures exposed to severe marine environments, Cem. Concr. Res. 39(11) (2009) 1068-1076.

[4] D.J. Shen, S.X. Wu, Experimental study and analysis on the mechanical performance of corroded reinforcement concrete beams in atmospheric environment, China Civil Eng. J. 8 (2009). (in Chinese)

[5] M. Valipour, M. Shekarchi, P. Ghods, Comparative studies of experimental and numerical techniques in measurement of corrosion rate and time-to-corrosion-initiation of rebar in concrete in marine environments, Cem. Concr. Compos. 48 (2014) 98-107.
[6] W. Zhu, R. François, Corrosion of the reinforcement and its influence on the residual structural performance of a 26-year-old corroded RC beam, Constr. Build. Mater. 51 (2014) 461-472.
[7] W. Zhu, R. François, C. Zhang, D. Zhang, Propagation of corrosion-induced cracks of the RC beam exposed to marine environment under sustained load for a period of 26 years, Cem. Concr. Res. 103 (2018) 66-76.
[8] C. Fu, N. Jin, H. Ye, X. Jin, W. Dai, Corrosion characteristics of a 4-year naturally corroded reinforced concrete beam with load-induced transverse cracks, Corros. Sci. 117 (2017) 11-23.
[9] Z.H. Lu, Y.B. Ou, Y.G. Zhao, C.Q. Li, Investigation of corrosion of steel stirrups in reinforced concrete structures, Constr. Build. Mater. 127 (2016) 293-305.
[10] P. Ghods, O.B. Isgor, J.R. Brown, F. Bensebaa, D. Kingston, XPS depth profiling study on the passive oxide film of carbon steel in saturated calcium hydroxide solution and the effect of chloride on the film properties, Appl. Surf. Sci. 257(10) (2011) 4669-4677.
[11] P. Ghods, O. Burkan Isgor, F. Bensebaa, D. Kingston, Angle-resolved XPS study of carbon steel passivity and chloride-induced depassivation in simulated concrete pore solution, Corros. Sci. 58 (2012) 159-167.
[12] M. Liu, X. Cheng, X. Li, Y. Pan, J. Li, Effect of Cr on the passive film formation mechanism of steel rebar in saturated calcium hydroxide solution, Appl. Surf. Sci. 389 (2016) 1182-1191.
[13] D. Song, J. Jiang, W. Sun, H. Ma, J. Zhang, Z. Cheng, et al., Effect of chromium micro-alloying on the corrosion behavior of a low-carbon steel rebar in simulated concrete pore solutions, J. Wuhan Univ. Technol.-Mater. Sci. Ed. 32(6) (2017) 1453-1463.
[14] M. Liu, X. Cheng, X. Li, Z. Jin, H. Liu, Corrosion behavior of Cr modified HRB400 steel rebar in simulated concrete pore solution, Constr. Build. Mater. 93 (2015) 884-890.
[15] F. Tang, G. Chen, R.K. Brow, J.S. Volz, M.L. Koenigstein, Corrosion resistance and mechanism of steel rebar coated with three types of enamel, Corros. Sci. 59 (2012) 157-168.
[16] H. Zheng, J.G. Dai, C.S. Poon, W. Li, Influence of calcium ion in concrete pore solution on the passivation of galvanized steel bars, Cem. Concr. Res. 108 (2018) 46-58.
[17] M. Farhadian, K. Raeissi, M.A. Golozar, S. Labbaf, T. Hajilou, A. Barnoush, Electrophoretic deposition and corrosion performance of Zirconia-Silica composite coating applied on surface treated 316L stainless steel: Toward improvement of interface structure, Surf. Coat. Technol. 380 (2019) 125015.

[18] L. Li, A. Sagues, Chloride corrosion threshold of reinforcing steel in alkaline solutions—effect of specimen size, Corros. 60(2) (2004) 195-202.
[19] C. Dehghanian, Study of surface irregularity on corrosion of steel in alkaline media, Cem. Concr. Res. 33(12) (2003) 1963-1966.
[20] E. Volpi, A. Olietti, M. Stefanoni, S.P. Trasatti, Electrochemical characterization of mild steel in alkaline solutions simulating concrete environment, J. Electroanal. Chem. 736 (2015) 38-46.
[21] J. Shi, W. Sun, J. Jiang, Y. Zhang, Influence of chloride concentration and pre-passivation on the pitting corrosion resistance of low-alloy reinforcing steel in simulated concrete pore solution, Constr. Build. Mater. 111 (2016) 805-813.
[22] H. Zheng, J.G. Dai, L. Hou, G. Meng, CS. Poon, W. Li, Enhanced passivation of galvanized steel bars in nano-silica modified cement mortars, Cem. Concr. Compos. 111 (2020) 103626.
[23] H. Zheng, C.S. Poon, W. Li, Mechanistic study on initial passivation and surface chemistry of steel bars in nano-silica cement pastes, Cem. Concr. Compos. 112 (2020) 103661.
[24] I.H. Toor, M. Ejaz, H.S. Kwon, Mott–Schottky analysis of passive films on Cu containing Fe–20Cr–xCu (x=0, 4) alloys, Corros. Eng. Sci. Technol. 49(5) (2014) 390-395.
[25] I.H. Toor, Mott-Schottky Analysis of Passive Films on Si Containing Stainless Steel Alloys, J. Electrochem. Soc. 158(11) (2011) C391.
[26] H. Jang, H. Kwon, In situ study on the effects of Ni and Mo on the passive film formed on Fe–20Cr alloys by photoelectrochemical and Mott–Schottky techniques, J. Electroanal. Chem. 590(2) (2006) 120-125.
[27] J. Williamson, O.B. Isgor, The effect of simulated concrete pore solution composition and chlorides on the electronic properties of passive films on carbon steel rebar, Corros. Sci. 106 (2016) 82-95.
[28] H. Zheng, J.G. Dai, W. Li, CS. Poon, Influence of chloride ion on depassivation of passive film on galvanized steel bars in concrete pore solution, Constr. Build. Mater. 166 (2018) 572-580.
[29] L. Hamadou, A. Kadri, N. Benbrahim, Characterisation of passive films formed on low carbon steel in borate buffer solution (pH 9.2) by electrochemical impedance spectroscopy, Appl. Surf. Sci. 252(5) 2005 1510-1519.
[30] S.J, Ahn, H.S. Kwon, Effects of solution temperature on electronic properties of passive film formed on Fe in pH 8.5 borate buffer solution, Electrochim. Acta. 49(20) (2004) 3347-3353.

[31] H.H. Ge, G.D. Zhou, W.Q. Wu, Passivation model of 316 stainless steel in simulated cooling water and the effect of sulfide on the passive film, Appl. Surf. Sci. 211(1-4) (2003) 321-334.
[32] A. Simoes, M. Ferreira, B. Rondot, M. da Cunha Belo, Study of passive films formed on AISI 304 stainless steel by impedance measurements and photoelectrochemistry, J. Electrochem. Soc. 137(1) (1990) 82.
[33] Y. Zhao, T. Pan, X. Yu, D. Chen, Corrosion inhibition efficiency of triethanolammonium dodecylbenzene sulfonate on Q235 carbon steel in simulated concrete pore solution, Corros. Sci. 158 (2019) 108097.
[34] M. Carmezim, A. Simoes, M. Montemor, M.D.C. Belo, Capacitance behaviour of passive films on ferritic and austenitic stainless steel, Corros. Sci. 47(3) (2005) 581-591.
[35] M. Liu, X. Cheng, G. Zhao, X. Li, Y. Pan, Corrosion resistances of passive films on low-Cr steel and carbon steel in simulated concrete pore solution, Surf. Interface Anal. 48(9) (2016) 981-989.
[36] D.G. Li, Y.R. Feng, Z.Q. Bai, J.W. Zhu, M.S. Zheng, Influence of temperature, chloride ions and chromium element on the electronic property of passive film formed on carbon steel in bicarbonate/carbonate buffer solution, Electrochim. Acta. 52(28) (2007) 7877-7884.
[37] N. Etteyeb, X.R. Nóvoa, Inhibition effect of some trees cultivated in arid regions against the corrosion of steel reinforcement in alkaline chloride solution, Corros. Sci. 112 (2016) 471-482.
[38] Z.H. Dong, W. Shi, G.A. Zhang, X.P. Guo, The role of inhibitors on the repassivation of pitting corrosion of carbon steel in synthetic carbonated concrete pore solution, Electrochim. Acta. 56(17) (2011) 5890-5897.
[39] K. Videm, R. Myrdal, Electrochemical behavior of steel in concrete and evaluation of the corrosion rate, Corros. 53(9) (1997) 734-742.
[40] G59-14 A. Standard Test Method for Conducting Potentiodynamic Polarization Resistance Measurements. ASTM International 2014.